Current oscillations in thin metal–oxide–semiconductor structures observed by ballistic electron emission microscopy

H. J. Wen[a] and R. Ludeke[b]
IBM T. J. Watson Research Center, Yorktown Heights, New York 10598

Andreas Schenk
Integrated Systems Laboratory, Swiss Federal Institute of Technology, CH-8092 Zürich, Switzerland

(Received 21 January 1998; accepted 11 May 1998)

Quantum interference oscillations of electrons in a thin SiO_2 layer were observed by ballistic electron emission microscopy (BEEM). With BEEM, electrons are injected across the gate of a metal–oxide–semiconductor (MOS) structure and directly into the conduction band of the SiO_2. The MOS capacitor consisted of a 5 nm thick Pd film deposited on a 2.8±0.2 nm oxide thermally grown on Si(100). Oscillations with up to four peaks in an energy range of 0–3 eV above the injection threshold were noted. Their magnitude is of the order of 30% of the underlying BEEM current. The oscillations were most salient and their energy location repeatable at points of the sample that were previously not exposed to the electron beam. Even modest exposures caused a buildup of positive charge. This charge resulted in energy shifts, as well as a weakening of the oscillations, both of which are a consequence of the added scattering and local field inhomogeneities associated with the random distribution of the positive charge. Solutions of the Schrödinger equation that included a built-in oxide potential of 0.20 V and image force effects at both interfaces gave excellent fits to the experimental data for an effective electron mass in the oxide $m_{ox}=0.63 \pm 0.09 m_o$. The uncertainty in m_{ox} arises from an uncertainty of ±0.2 nm in the determination of the oxide thickness by ellipsometric methods. Nevertheless, the obtained value is well above the generally accepted value of $0.5 m_o$. © *1998 American Vacuum Society.* [S0734-211X(98)05804-1]

I. INTRODUCTION

The notion that electron wave interference should occur in Fowler–Nordheim (FN) tunneling of electrons into thin (<6 nm) oxide layers comprising a metal–oxide–semiconductor (MOS) structure was proposed by Gundlach over three decades ago.[1] Oscillations in the (oxide)-bias-dependent current arise from the interference of electron waves reflected at the oxide–semiconductor (OS) interface and at the point of emergence of the tunneling electrons at the bottom of the tilted SiO_2 conduction band. The latter point is a ''hard'' turning point, whereas the OS interface is relatively transparent, with reflections occurring mainly from the wave-function mismatch across the interface. Experimental verification of a weak oscillatory structure in the FN current was reported by Maserjian and Petersson in 1974,[2,3] and by others in subsequent years.[4–8] Invariably, these data were analyzed in terms of Gundlach's theory based on a trapezoidal barrier (i.e., neglecting image force effect),[1] from which an estimation of the conduction-band effective mass m_{ox} of SiO_2 can be made. Values for m_{ox} ranged from $0.32 m_o$ (Ref. 1) to as high as $0.85 m_o$,[2,6] where m_o is the free-electron mass. The conduction-band effective mass was estimated as well from fits of the theoretical FN current to experimental data covering many orders of magnitude of the current. Again, image force effects were neglected and values reported ranged from a low of $0.3 m_o$ (Ref. 9) to $0.5 m_o$.[10] When image forces were included, the values were somewhat higher.[11,12] Although a defacto value of $0.5 m_o$ is almost exclusively used in transport simulations,[13] the reported discrepancies in m_{ox} and its dependence on fitting assumptions questions the acceptance of this standard, and prompts one to look for alternative experimental methods to extract a value for m_{ox}. Intrinsically, interference phenomena represent the most straight forward method to arrive at a value of m_{ox}, provided the inherent difficulties in the experiment and simulation of FN tunneling can be overcome. These include a position-dependent energy of the electron, uncertain tunneling (injection) description, a weak signal superimposed on a strongly rising current and averaging effects due to a large and often inhomogeneous device area. These constraints, as we shall see, can be circumvented by using the local injection scheme of ballistic electron emission microscopy (BEEM). This scanning tunneling microscope (STM) based method allows the injection of variable energy and nearly monochromatic electrons into the thin gate of a MOS structure and then directly into the conduction band of the SiO_2.[14] Both the high lateral confinement (<2 nm) of the injected electrons in thin oxides (<4 nm),[15] which enhances the attainment of a homogeneous local oxide potential, and the relatively weak power dependency on energy for the transmitted current are contributory to the realization of pronounced interference oscillations. Moreover, the modeling of transport in SiO_2 for ''over the barrier'' injection depends on fewer unknowns than FN and direct tunneling, which assures a higher degree of confidence in the calculated parameters obtained through fits to the data. We present here both oscillatory BEEM current data for a 2.8 nm SiO_2 layer and fits

[a] Present address: IBM Austin Research Laboratory, Austin, TX 78758.
[b] Corresponding author; electronic mail: ludeke@watson.ibm.com

using solutions of the Schrödinger equation that include image force effects, with the relevant adjustable parameter being the effective mass m_{ox} and oxide thickness d. With the assumption that d is known within ±0.2 nm, a ''best-fit'' value of $m_{ox}=0.63\pm0.09m_o$ was obtained. Uncertainties in other parameters needed for the fits, such as the built-in oxide potential V_{ox} and the effective dielectric constant ϵ_{ox} proved to be of minor consequence to the error in m_{ox}.

II. EXPERIMENTAL DETAILS

A. Ballistic electron emission microscopy (BEEM)

BEEM is an adaptation of the conventional STM and is characterized by a special sample configuration that consists of a thin conducting layer, usually a metal, deposited on top of the semiconductor structure to be measured. Although historically a Schottky barrier, here the sample is a MOS structure. The metal provides a ground contact relative to which both the STM tip bias V_T and the applied oxide bias V_b are referenced. The tip bias thus defines the energy eV_T of the electrons injected into the metal. For metal film thicknesses comparable or less than the electron mean-free path, most of the electrons will traverse the metal and reach the far interface without scattering (ballistically). If the electrons encounter a potential barrier at that interface, they will backscatter unless their energy exceeds that of the metal–oxide barrier. In this case, a fraction of the electrons will be injected into the conduction band of the SiO_2. Here, they may undergo electron–phonon scattering, which may cause some of them to return to the metal.[14] The remainder, if not trapped,[16,17] proceed towards the Si substrate to emerge as a collector current I_c. The STM is operated under constant I_T conditions. For the experiments reported here $I_T=2$ nA. In the spectroscopy mode of BEEM, the STM image acquisition is interrupted at a predetermined point on the surface and the collector current I_c is measured as V_T is ramped over a voltage range that includes the barrier potential. Initially, I_c is zero until V_T exceeds a threshold value V_o that represents the maximum in the barrier potential of the MOS structure.

An energy-band diagram for a BEEM experiment on a MOS structure is schematically shown in Fig. 1 for $V_b=0$. The curved leading edge of the oxide barrier results from the inclusion of image force lowering,[18] a corresponding, but weaker effect at the SiO_2–Si interface was omitted for clarity. Conditions for injection into the conduction band of the SiO_2 are shown ($V_T>V_o$). The threshold for injection V_o is about 4 V in the absence of a negative trapped charge.[17] The application of an external oxide bias V_b further modifies the electron energies as they move across the oxide. In the present experiments $V_b=0$, however, $V_{ox}\approx0.2$ V due to work-function differences between the n-type Si and the Pd layer.[18] It is worth pointing out that the energy distribution of electrons injected by the STM tip fall off in near-exponential fashion from its maximum value, with an energy spread that decreases with increasing energy eV_T. A theoretical full width at half maximum of ~0.150 eV was estimated for $eV_T=6$ eV.[19] This energy spread is sufficiently monochromatic for characterizing most hot electron phenomena in oxides.

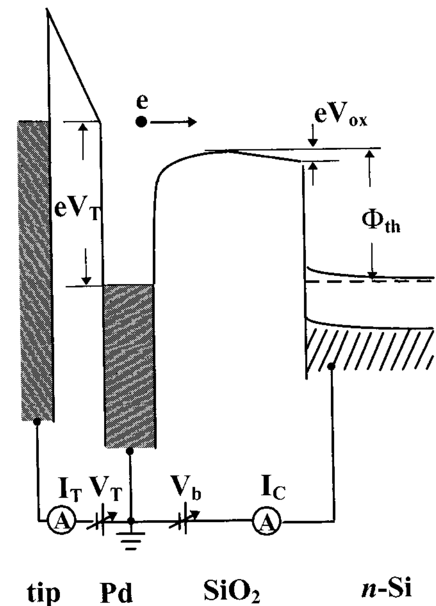

FIG. 1. Energy-band diagram of a BEEM experiment applied to a MOS structure. V_T is the STM tip bias that determines the energy eV_T of the electrons injected by the tip into the Pd metal gate. An optional oxide bias V_b may also be applied. Here, $V_b=0$. The oxide potential V_{ox} shown is attributable to work-function differences between Pd and n-Si, $V_{ox}\approx0.2$ V in the absence of oxide charge.

B. Sample preparation

The device-grade SiO_2 layers were thermally grown near 800 °C in dry oxygen on 125 mm Si(100) wafers doped in the low 10^{17} cm^{-3} range. The wafer was subsequently annealed in forming gas at 500 °C. Working samples of ~8 $\times$15 mm^2 were cleaved from the wafers and introduced into the ultrahigh vacuum (UHV) preparation chamber, where they were outgassed over night at ~200 °C to desorb water and other surface contaminants. The sample was then transferred under UHV to the metal deposition chamber, where Pd dots 0.2 mm in diameter were thermally evaporated onto the SiO_2 through a shadow mask. The substrate was held near 30 K during deposition in order to smooth the surface morphology of the thin (~5 nm) Pd films. This process produced films with a nodular structure, typically, 8 nm in diameter that protruded <2 nm above the valleys.[17] A smooth surface morphology is desirable to reduce BEEM image contrast arising from the surface topography of the metal.[14] The finished sample was allowed to warm up to room temperature and was then transferred under UHV into the STM chamber. The grounding contact was carefully positioned onto a selected Pd dot by means of three orthogonally mounted Inchworms™. STM images and sets of BEEM spectra were then taken. Typically, 9–25 BEEM spectra were measured in a grid pattern covering 25×25 to 50×50 nm^2 areas. As will become apparent in the next section, it is desirable to widely separate the acquisition points for each spectrum to avoid charging effects arising from electrons in-

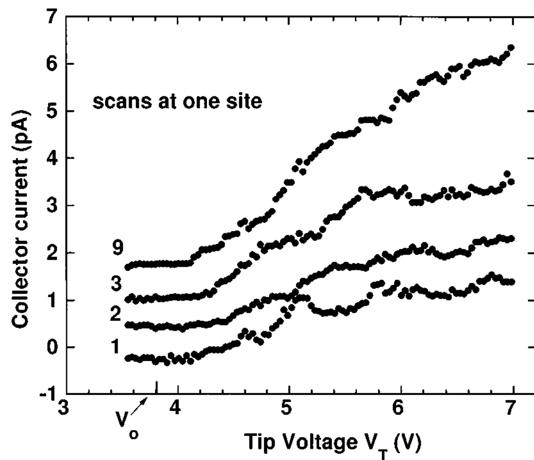

FIG. 2. Single scan BEEM spectra on a 5 nm Pd/2.8 nm SiO_2/n-Si(100) MOS structure measured at the same point on the sample. The numerals indicate the number of the scan. The first spectrum was taken on a previously unexposed area of the sample. V_0 marks the current threshold bias, obtained by computer-aided fits. The spectra are vertically displaced for clarity. $I_T = 2$ nA, $V_b = 0$ V.

jected at a prior location and then scattered into the area to be probed. In order to study charging effects, sequential spectra were acquired at the same location of the sample. Although spectral acquisition times are of the order of 10 s, tip drifts were of the order 0.1 nm/min, which assured that injections occurred at the same point of the sample.

The oxide thickness was determined by spectroscopic ellipsometry on two different instruments operating at a 632.8 nm wavelength. The thickness measured by both instruments agreed within 0.3 nm. We found that outgassing the sample in UHV at ~200 °C prior to the measurement in the same stage and conditions as the BEEM samples prior to metallization, reduced the measured thickness by ~0.3 nm. The difference was attributed to adsorbed contaminants. The value for $d = 2.8 \pm 0.2$ nm was the best estimate for the oxide thickness after the anneal and was used in the simulations. In unpublished studies at IBM, the oxide thickness determined by C–V methods on oxides of comparable thickness, after correction for polydepletion and quantization effects, was, in general, ~0.2–0.3 nm thinner than that obtain with the ellipsometer.[20] Consequently, the value quoted above, except for instrument error, most likely represents a slight overestimate in the thickness.

III. COLLECTOR CURRENT OSCILLATIONS

A sequence of single spectral scans taken at the same point of the 5 nm Pd/2.8 SiO_2/Si(100) sample is shown in Fig. 2. The digits next to the curves indicate the number of the spectral scan. The first scan shows a strong modulation of the collector current that progressively broadens and weakens as the number of scans increases. The oscillatory structure is attributed to quantum interference effects in the thin SiO_2 layer, which arise from the constructive/destructive interference of electron waves reflected at the metal–SiO_2 and SiO_2–Si boundaries of the SiO_2 ''cavity.'' In the simplest realization, transmission maxima follow the quantization condition: $E = (n\pi\hbar/d)^2/2m^*$ $(n = 1,2,3,...)$, where E is the electron energy, d the cavity width, and m^* the effective electron mass.[1] No oscillatory structure due to the metallic film was ever observed by us, a failure that we attribute to the uneven nodular character of the Pd film.[17,21] The oscillatory structure in the first scan of Fig. 2 is repeatable provided the scan is made on a new, previously unexposed point of the sample. However, only about 1/3 of the virgin points yielded a spectral structure with similar periodicities; the remainder lacked the oscillatory structure entirely or exhibited a weak and smeared out structure of varying periodicities. After a number of scans, shown here at the ninth, the structure is altered and strongly suppressed. A second point to be noted is the progressive increase in the collector current with each scan. Such increases were previously observed,[21] and were attributed to the buildup of stress-induced positive charge near the anode (OS interface). Although for thicker oxides ($d > 4$ nm) electrons are trapped in the oxide, resulting in an increase in V_o and a decrease I_c, for thinner oxides the electrons leak out, thereby revealing the presence of the positive charge.[17] Its presence at the anode has a small effect (<0.1 V) on V_o, primarily due to image force lowering, that is consistent with our observations (~0.05 V). Yet, the positive charge creates an accelerating field that, again with the inclusion of image force effects, results in an enhancement of transmission probabilities and an increase in I_c.[22] Since the positive charge is randomly distributed, its buildup during the scans progressively distorts the local potential the electrons see as they traverse the oxide. Such potential fluctuations affect the ability of the electron waves to interfere coherently.

The oscillatory structure commonly observed on a virgin portion of the surface, such as the bottom curve in Fig. 2, exhibits peaks for $V_T \approx 4.6$, 5.1, 5.8, and 6.8 V. We have limited ourselves to $V_T < 7$ V to minimize hot electron damage. We also convinced ourselves that an additional weak peak appears near 4.1 V, but is not readily discernible in an average spectrum because of the background noise. It should be realized that less than 1 in 1000 electrons injected by the STM tip are collected in the Si substrate. The oscillatory structure is also shown in Fig. 3, where we have averaged spectra from five data sets. The observation of pronounced oscillation due to quantum interference effects is at first somewhat surprising, since the ''cavity'' of the SiO_2 film is quite leaky, with allowed states in both cladding regions (metal and Si) expected to reduce the reflectivity at the interfaces. Moreover, the extensive electron–phonon scattering in SiO_2, with a mean-free path of 1–2 nm that is, typically, less than the SiO_2 film thickness,[14,23] is expected to further suppress the interference oscillations. Of course, interference oscillations have been observed, albeit weak, in MOS capacitors using the FN injection method.[2–7] Support for the correctness of this interpretation also comes from the theoretical modeling that will be described next. Compared to the early work by Gundlach[1] for over the barrier interference, the present work incorporates image force effects, which

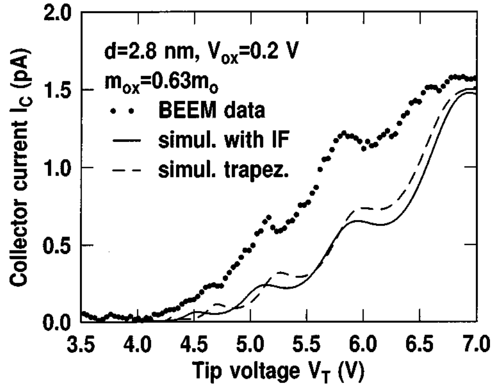

FIG. 3. Composite BEEM spectrum of five sets of data, each taken on a previously unexposed location of a 5 nm Pd/2.8 nm SiO_2/n-Si(100) MOS capacitor. The solid line represents the best fit of the peak location to the data using theoretical transmission coefficients calculated with the indicated parameters and with image force effects included. The dashed curve was obtained by omitting the image force effects.

represent the screening of the electrons in SiO_2 by nearby conduction electrons in the metal and Si. We will fit the theoretical curves to our data and extract from it the relevant parameter of the effective conduction-band mass m_{ox} of SiO_2.

IV. THEORETICAL TRANSMISSION COEFFICIENTS

The transmission coefficient (TC) $T(E)$ was calculated by a numerical solution of the one-dimensional Schrödinger equation assuming an idealized potential barrier with (i) the classical image potential, (ii) its divergencies removed as discussed below, (iii) neglecting oxide charges, and (iv) using the optical dielectric constant of the present thin SiO_2 layer. For dispersion in the latter, we assumed a parabolic *E(k)* relation with an effective mass m_{ox} as parameter. The barrier was discretized by *N* partial subbarriers of rectangular shape which covered the whole oxide layer of thickness *d*. From the continuity of wave-function and quantum-mechanical current density at each boundary, the TC is then found by (see, e.g., Ref. 24)

$$T(E)=\frac{m_0}{m_{N+1}}\frac{k_{N+1}}{k_0}\frac{|\det M|^2}{|M_{22}|^2}, \tag{1}$$

where M is a (2×2) product matrix $M=\Pi_{l=0}^{N}M_l$ with transfer matrices M_l given by

$$M_l=\frac{1}{2}\begin{vmatrix}(1+S_l)\exp[-i(k_{l+1}-k_l)x_l] & (1-S_l)\exp[-i(k_{l+1}+k_l)x_l]\\ (1-S_l)\exp[+i(k_{l+1}+k_l)x_l] & (1+S_l)\exp[+i(k_{l+1}-k_1)x_l]\end{vmatrix}. \tag{2}$$

In Eq. (2) $S_l=m_{l+1}k_l/(m_lk_{l+1})$, and the effective masses and momenta are discretized as $m_l=m^*[(x_{l-1}+x_l)/2]$ and $k_l=k[(x_{l-1}+x_l)/2]$, respectively, x_l being the position of the lth boundary. If the metal–oxide interface is at x_0 and the oxide–silicon interface at x_N, then $m_o=m_M$ denotes an effective mass in the metal electrode and $m_N=m_{Si}$ an ''effective'' mass in silicon. For all other l we have $m_l=m_{ox}$. Because of the assumed parabolic dispersion within the oxide, the momentum takes the form

$$k(x)=\sqrt{2m_{ox}/\hbar^2}\sqrt{E-[\Phi_B+eF_{ox}x+E_{im}(x)]}, \tag{3}$$

there, with the image potential[25]

$$E_{im}(x)=-\frac{e^2}{16\pi\epsilon_{ox}}\sum_{n=0}^{\infty}(-\kappa)^n \times\left[\frac{1}{nd+x}-\frac{\kappa}{d(n+1)-x}+\frac{2\kappa}{d(n+1)}\right], \tag{4}$$

which includes the effect of all images in the two electrodes. In Eq. (4) κ is given by $\kappa=(\epsilon_{ox}-\epsilon_{Si})/(\epsilon_{ox}+\epsilon_{Si})$. The remaining quantities are the metal–SiO_2 barrier height for electrons Φ_B, the built-in potential drop over the oxide layer $eF_{ox}x$, and the dielectric constants ϵ_{ox} and ϵ_{Si} in oxide and silicon, respectively. Neglecting the image force, $T(E)$ can be written analytically in terms of Airy functions as was first done by Gundlach.[1] In our simulations we used the following parameters: $d=2.8$ nm, $N=30$, $\Phi_B=4.1$ eV, $F_{ox}=V_{ox}/d=-0.071\,43$ V/nm (potential peak at the oxide–metal boundary), $m_{Si}=0.19m_o$, $m_M=m_o$, $\epsilon_{Si}=11.7$, and $\epsilon_{ox}=2.13$.

The significance of the ''classical'' image force in tunneling experiments was supported by Binnig *et al.*[26] They showed that it is indispensable in order to describe correctly the barrier-width dependence and absolute value of the vacuum tunnel current. The existence of image force effects for over the barrier transport in MOS structures was also shown recently by Wen *et al.*[18] On the other hand, the ''classical'' form can only be used asymptotically, i.e., a few Bohrs off the image plane. In the vicinity of that plane, the classical singularity has to be replaced by a self-consistent potential shape.[27] This shape is smooth throughout the interface and can be modeled by a smooth variation of the dielectric constant.[28] For simplicity, we have removed the singularity of the classical image potential in a more simplistic way by a straight continuation of both, the band edge in the semiconductor and the gate Fermi level.

The simulations involve further simplifications. Any possible band-structure mismatch at the Si–SiO_2 interface was disregarded. In above-barrier transitions electrons tunnel into highly excited states in the silicon near the Si–SiO_2 boundary. Here, the ''effective'' mass m_{Si} is merely a fitting parameter. Fortunately, m_{Si} only enters the preexponential factor of the TC and has no significant influence on the

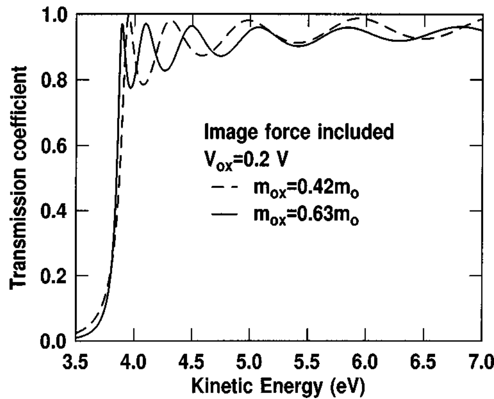

FIG. 4. Calculated transmission coefficients, image force effects included, for $m_{ox}=0.63m_0$ (solid line) and $m_{ox}=0.42m_0$ (dashed line), with the remaining parameters determined from experiment. The solid line was used to determine the best fit in Fig. 3.

interpretation of the measurements. The missing knowledge about the band structure of the ultrathin SiO_2 layer is covered by the ''tunneling'' mass m_{ox}. This parameter can be adjusted when the oscillations of the simulated TC are brought in coincidence with the periodicity of the measured current.

Results of the calculation for the selected parameters are shown in Fig. 4 (solid line). The transmission coefficient $T(E)$ exhibits initially a strong oscillatory structure whose period increases and whose amplitude decreases with energy. Although a barrier of $\Phi_B=4.1$ eV was used, the transmission threshold is closer to 3.9 eV. The decrease is consistent with experimental observations and predictions of image force theory, based on thicker oxides,[18] for the image force lowering expected for a 2.8 nm oxide and $V_{ox}=0.2$ V. *T(E)* is actually finite at energies <3.5 eV, which is a consequence of electrons tunneling through the rounded barrier near its top (see Fig. 1). The effect on the oscillatory structure of a change in the electron mass is illustrated by the dashed curve in Fig. 4, for which $m_{ox}=0.42m_o$, all other parameters remaining the same. A lower mass increases the effective wavelength of the electron for a given energy, which thereby requires a larger value to ''fit'' the wavelength into the cavity. Hence, the periodicity increases, as it also would by decreasing the cavity width (oxide thickness). The lighter electron mass also enhances the probability for the electron to tunnel through the top of the barrier, as indicated by the increased intensity of the tail in *T(E)* near 3.5 eV.

V. DISCUSSION AND CONCLUSIONS

To fit the theoretical transmission function to the experimental data either a corresponding function should be derived from experiment or the experimental collector current should be simulated. Neither is, at present, a realizable option due to the complexity of the transmission process of hot electrons through a MOS structure. Certain inelastic aspects of transmission across the oxide have been simulated by Monte Carlo calculations.[14,15] However, the role of transport across the metal, scattering at the interfaces, including details of the band structures, have generally been ignored. And this for good reason, as much of this information is neither available, nor calculable within the framework of present knowledge of the structurally incoherent system that the MOS structure represents.

As BEEM spectra in general exhibit little structure and obey, at least near threshold, a power-law dependence of the collector current I_c on V_T,[29] we can attempt to represent the BEEM spectra by multiplying the transmission coefficient with a simple quadratic power law, i.e., $I_c \propto (V_T - V_o)^2$. The result is shown for $V_o=3.9$ V and $T(E)$ calculated with $m_{ox}=0.63m_o$ and with image forces included in Fig. 3 as a solid line. As can be ascertained, an energy-independent $m_{ox}\approx 0.63m_o$ is sufficient for a reasonable fit over the entire voltage range. No attempt has been made to make the curves overlap, but merely to show the position of the structure. The sensitivity of the structure on m_{ox} (aside from that shown in Fig. 4) can be estimated from differentiating the quantization condition $E=(n\pi\hbar/d)^2/2m^*$. Thus, $\delta m_{ox}=-(\delta E/E)m_{ox}$, with a change in the peak location, let us say near 6 eV, of 0.1 eV resulting in a $\delta m_{ox}=0.01m_o$. Thus, a conservative estimate of the error gives a best-fit value of $m_{ox}=0.63 \pm 0.02m_o$. In contrast, the error in d of ± 0.2 nm yields a substantially larger uncertainty of $\pm 0.09m_o$. Other uncertainties due to a lack of knowledge in $V_{ox}(<\pm 0.1\text{ V})$ or choice of ϵ_{ox} give uncertainties of $<0.01m_o$, so that our present best estimate for m_{ox} is $m_{ox}=0.63\pm 0.09m_o$.

Also shown in Fig. 3 is the dashed curve generated with a *T(E)* calculated with a trapezoidal barrier, i.e., with the omission of image force effects, but otherwise with identical parameters as the solid curve. The latter clearly gives a better fit to the data. Ignoring image force effects and optimizing the fit to the experimental data yield a $m_{ox}\approx 0.65m_o$. However, we find no physical reason to ignore image force effects, but merely show its role, having been motivated to show it by reason of a consistent historical neglect of image force effects by most practitioners of the art of electrical characterization of MOS structures.

The consequence of omission of image force effects is rather small on the magnitude of m_{ox}, however, its inclusion has a dramatic effect on the transmission coefficient in the presence of an oxide field. This is illustrated for relatively moderate fields in Fig. 5. The lowering of the threshold for increasing V_{ox} is clearly observable, with an accompanying expansion of the period for low n values (i.e., initial periodicity for $V_{ox}=0$ is less than that for $V_{ox}>0$). It is interesting to note that for $V_{ox}=1$ V the weak first peak corresponds to electrons partially tunneling through the top of the barrier before interference occurs (somewhat akin to the FN case). The rapid shifting of the structure for even moderate fields clearly suggests that in the presence of field inhomogeneities on the local sampling scale the observation of the interference effect would be quickly suppressed. In our experiment, positive charge near the anode is (randomly) generated, a conclusion also reached from other stressing experiments $(I-V)$ on MOS capacitor structures.[30] Even a single charge would generate a field of order 1 V/nm at the injecting point of the SiO_2 layer. Even at a distance of several nanometers

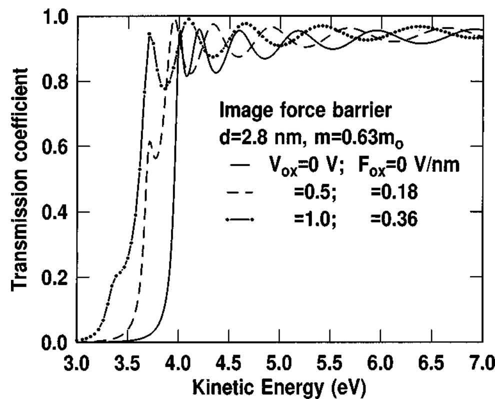

FIG. 5. Oxide field dependence of transmission coefficients calculated with the best-fit parameters, excepting V_{ox}. Image force effects are included.

away the resulting fields are comparable or larger than those in the simulations of Fig. 5. Because of scattering at the interfaces and in the SiO_2, electrons will experience somewhat different paths. Consequently, electrons injected locally near an area of charge would experience both a local- and time-dependent variation of the fields, which leads to a suppression of the interference effects, as was observed in our time-dependent experiments (Fig. 2). Thus, a condition for the observation of quantum interference is a region essentially free of oxide charge. The lateral extent of this region can only be guestimated from our observation that we needed to move at least 10 nm away from any point of prior exposure (and hence, positive charge buildup) before we could observe a new oscillatory structure in the BEEM spectrum. The fact that a virgin area did not necessarily lead to the observation of quantum interference suggests that the presence of local charge was quite pervasive. Since device quality oxides have generally quite low densities of defects, traps, etc. ($<10^{11}/cm^2$), it appears somewhat surprising that we do not observe quantum interference most of the time. Two reasons for this failure may be sited: (a) Pd metallization induces a large ($\sim 10^{13}/cm^2$) density of electron traps,[17] and (b) multiple scattering in the metal and SiO_2 layer can effectively broaden the sampling area. Although no net electron charge has been observed in the thin layers used here, electrons can nevertheless momentarily be trapped before leaking out by tunneling to the electrodes.[21] A trapped electron acts as a scattering center and distorts the field sensed by the other electrons passing in its vicinity.

We have shown here that direct electron injection into a laterally confined area of a MOS structure can lead to the observation of strong quantum interference oscillations. A theoretical analysis yields an effective conduction-band mass of $0.63m_o$, and further reveals an extreme sensitivity of the oscillatory structure to the oxide thickness and the oxide field. The technique has, thus, the potential of an extremely sensitive local probe to address issues of local structural and electric homogeneity, issues of great importance in the area of future ultrasmall devices. It is to be expected that the use of polygates with their drastically lower density of trap states would considerably enhance the observation of quantum interference in thin oxides, and thereby facilitate the realization of this technique as a potentially powerful local probe to assess dielectric quality.

[1]K. H. Gundlach, Solid-State Electron. **9**, 949 (1966).
[2]J. Maserjian and G. P. Peterson, Appl. Phys. Lett. **25**, 50 (1974).
[3]J. Maserjian, J. Vac. Sci. Technol. **11**, 996 (1974).
[4]M. V. Fischetti, D. J. DiMaria, L. Dori, J. Batey, E. Tierney, and J. Stasiak, Phys. Rev. B **35**, 4044 (1987).
[5]J. C. Poler, K. K. McKay, and E. A. Irene, J. Vac. Sci. Technol. B **12**, 88 (1994).
[6]S. Zafar, K. A. Conrad, Q. Liu, E. A. Irene, G. Hames, R. Kuehn, and J. J. Wortman, Appl. Phys. Lett. **67**, 1031 (1995).
[7]S. Zafar, Q. Liu, and E. A. Irene, J. Vac. Sci. Technol. A **13**, 47 (1995).
[8]H. S. Momose, M. Ono, T. Yoshitomi, T. Ohguru, S. Nakamura, M. Saito, and H. Iwai, IEEE Trans. Electron Devices **45**, 1233 (1996).
[9]T. Yoshida, D. Imafuku, J. L. Alay, S. Miyazaki, and M. Hirose, Jpn. J. Appl. Phys., Part 2 **34**, L903 (1995).
[10]Z. A. Weinberg, J. Appl. Phys. **53**, 5052 (1982).
[11]Reference 10 lists earlier results with image force effects included.
[12]A. Schenk and G. Heiser, J. Appl. Phys. **81**, 7900 (1997).
[13]M. V. Fischetti, S. E. Laux, and E. Crabbé, J. Appl. Phys. **78**, 1058 (1995), and references therein.
[14]R. Ludeke, A. Bauer, and E. Cartier, Appl. Phys. Lett. **66**, 730 (1995); J. Vac. Sci. Technol. B **13**, 1830 (1995).
[15]R. Ludeke, H. J. Wen, and E. Cartier, J. Vac. Sci. Technol. B **14**, 2855 (1996).
[16]B. Kaczer and J. P. Pelz, J. Vac. Sci. Technol. B **14**, 2864 (1996).
[17]H. J. Wen and R. Ludeke, J. Vac. Sci. Technol. B **15**, 1080 (1997).
[18]H. J. Wen, R. Ludeke, D. M. Newns, and S. H. Low, J. Vac. Sci. Technol. A **15**, 784 (1997).
[19]N. D. Lang, A. Yacoby, and Y. Imry, Phys. Rev. Lett. **63**, 1499 (1989); N. D. Lang (private communication).
[20]C. P. D'Emic (private communications).
[21]H. J. Wen and R. Ludeke, J. Vac. Sci. Technol. A **16**, 1735 (1998).
[22]R. Ludeke, E. Cartier, and H. J. Wen (unpublished results). The transmission probability here is the one associated with inelastic scattering events due to electron–phonon interactions, see Ref. 14 for further details.
[23]E. Cartier, D. Arnold, D. J. DiMaria, M. V. Fischetti, P. Braunlich, S. C. Jones, X. A. Shen, R. T. Casper, and P. J. Kelly, Rev. Solid State Sci. **5**, 531 (1991).
[24]Y. Ando and T. Itoh, J. Appl. Phys. **61**, 1497 (1987).
[25]M. Kleefstra and G. C. Herman, J. Appl. Phys. **51**, 4923 (1980).
[26]G. Binnig, N. Garcia, H. Rohrer, J. M. Soler, and F. Flores, Phys. Rev. B **30**, 4816 (1984).
[27]P. A. Serena, J. M. Soler, and N. Garcia, Phys. Rev. B **34**, 6767 (1986).
[28]F. Stern, Phys. Rev. B **17**, 5009 (1978).
[29]W. J. Kaiser and L. D. Bell, Phys. Rev. Lett. **60**, 1406 (1988); L. D. Bell and W. J. Kaiser, *ibid.* **61**, 2368 (1988).
[30]D. A. Buchanan, D. J. DiMaria, C.-A. Chang, and Y. Taur, Appl. Phys. Lett. **65**, 1820 (1994).